GREEN SYNTHESIS OF ZnO-CuO NANOCOMPOSITE FOR EFFICIENT ADSORPTION OF RHODAMINE B-DYE

Dissertation submitted to

Visvesvaraya National Institute of Technology, Nagpur

In partial fulfillment of the requirements for the award of the degree

Masters of science

in

Chemistry

by

Tejasvi Anil More (MS23CHM001)

Under the guidance of

Dr. Sangesh P. Zodape

Department Of Chemistry

Visvesvaraya National Institute of Technology

Nagpur- 440 010 (India)

May 2025

GREEN SYNTHESIS OF ZnO-CuO NANOCOMPOSITE FOR EFFICIENT ADSORPTION OF RHODAMINE B-DYE

Dissertation submitted to

Visvesvaraya National Institute of Technology, Nagpur

In partial fulfillment of the requirements for the award of the degree

Masters of science

in

Chemistry

by

Tejasvi Anil More (MS23CHM001)

Under the guidance of

Dr. Sangesh P. Zodape

Department Of Chemistry

Visvesvaraya National Institute of Technology

Nagpur- 440 010 (India)

May 2025

©Visvesvaraya National Institute of Technology (VNIT) 2025

Department of Chemistry

Visvesvaraya National Institute of Technology, Nagpur

Declaration

I, Tejasvi Anil More, hereby declare that this dissertation titled "Green synthesis of ZnO-CuO Nanocomposite for efficient adsorption of Rhodamine B-dye" is carried out by me in the Department of Chemistry of Visvesvaraya National Institute of Technology, Nagpur. The work is original and has not been submitted earlier whole or in part for the award of any degree/diploma at this or any other Institution/University.

Name and Signature

Date:

Certificate

This to certify that the dissertation titled "Green synthesis of ZnO-CuO Nanocomposite for efficient adsorption of Rhodamine B-dye" is submitted by **Tejasvi Anil More** in partial fulfillment of the requirements for the award of the degree of **Master of Science in Chemistry,** VNIT Nagpur. The work is comprehensive, complete and fit for final evaluation.

Dr. Sangesh P. Zodape

Assistant Professor

Department of Chemistry

VNIT, Nagpur

Head, Department of Chemistry,

VNIT, Nagpur

Date:

VISVESVARAYA NATIONAL INSTITUTE OF TECHNOLOGY, NAGPUR

Non-Plagiarism Certificate

Certified that M.Sc. Dissertation titled "Green synthesis of ZnO-CuO nanocomposite for efficient adsorption of rhodamine b dye" submitted by Tejasvi Anil More Enrollment No. MS23CHM001 ID No. 30066 has been checked for plagiarism using TURNITIN software and the overlap is found within the prescribed limits. A summary of the report is given below:

Tejasvi Anil More

MS23CHM001

Id. No. 30066

Dr. Sangesh P. Zodape

Assistant Professor

Department of Chemistry

VNIT, Nagpur

Acknowledgement

I would like to express my profound gratitude to my project supervisor, Dr. Sangesh P. Zodape, Department of Chemistry, for his encouragement and patience during the course of my M.Sc. project. I would like to express my sincere gratitude to the Dr. Sujit Kumar Ghosh, Head of the Department, Chemistry for their valuable support throughout the course of my thesis. I am very grateful for their guidance and disciplinary inspiration which has helped me to improve my personal skills. I extend my thanks to the Department of Chemistry, for providing the necessary facilities to undertake the project efficiently.

I convey my sincere gratitude to Ms. Sakshi Barad, Doctoral Fellow at VNIT, Nagpur for her constant support and guidance.

Finally, I would like to thank my family and friends whose constant support and blessings helped me throughout the project.

Tejasvi Anil More

(MS23CHM001)

ABSTRACT

GREEN SYNTHESIS OF ZnO-CuO NANOCOMPOSITE FOR EFFICIENT ADSORPTION OF RHODAMINE B DYE

Tejasvi Anil More (MS23CHM001) and Dr. Sangesh P. Zodape

In recent years, the development of environment friendly methods for synthesizing nanomaterials has gained significant attention due to the growing demand for sustainable and non-toxic approaches. In this study, a zinc oxide-copper oxide (ZnO-CuO) nanocomposite was successfully synthesized using an aqueous extract of lagenaria siceraria, commonly known as bottle gourd through green approach. The plant extract severed as a natural reducing and stabilizing agent, enabling the formation of the nanocomposite without the need for harmful chemical reagents. The prepared ZnO-CuO nanocomposite was characterized using an analytical techniques such as Scanning Electron Microscopy (SEM), X-ray Diffraction (XRD), Fourier Transform Infrared Spectroscopy (FTIR), UV-Visible Diffuse Reflectance Spectroscopy (UV-DRS), Brunauer-Emmett-Teller (BET) and Thermogravimetric Analysis (TGA). SEM revealed a porous and aggregated nanoparticle morphology, with average crystallite size of approximately 63.52 nm. The average crystallite size, determined using the Debye-Scherrer equation, was approximately 15.86 nm, suggesting a successful combination of both metal oxides at nanoscale with characteristic peaks corresponding to ZnO and CuO phases by XRD technique. FTIR indicates the presence of metal-oxygen bonds, as well as residual phytochemical groups from the plant extract. UV-DRS showed strong adsorption in the visible region and a calculated band gap of about 2.7 eV. BET surface area analysis revealed a specific surface area of 11.54 m^2/g, conforming the mesoporous structure and high surface reactivity of the nanocomposite. TGA was also performed to evaluate the thermal stability of the synthesized composite. The characterization confirmed the successful formation of a ZnO-CuO composite with nanoscale features and favourable textural properties. The synthesised material was tested for adsorption efficiency towards rhodamine B dye from aqueous solution. The composite exhibited excellent adsorption capacity, highlighting its potential as effective, low cost and eco-friendly adsorbent for wastewater treatment applications.

List of Figures

Serial No.	Title	Page No.
	Chapter 1	
1.1	Classification of Nanomaterials	8
1.2	Schematic Illustration of the Several Procedures Used to Produce Nanoparticles	8
1.3	Sources of Water Pollution	10
	Chapter 2	
2.1	Systematic Representation of the ZnO-CuO Nanocomposite Synthesis	16
	Chapter 3	
3.1	PXRD of ZnO-CuO Nanocomposite.	23
3.2	FTIR Analysis on ZnO-CuO.	27
3.3	(a), (b) and (c) SEM images of ZnO-CuO Nanocomposite	27
3.4	EDX Analysis.	27
3.5	(a),(b) and (c) Elemental Mapping of ZnO-CuO Nanocomposite.	28
3.6	a) UV-DRS spectra	29
	b) Tauc plot	29
3.7	(a) N_2 Adsorption-Desorption Isotherm	30
	(b) Pore Size Distribution of ZnO-CuO	30
3.8	Thermogravimetric Analysis	31
3.9	Optimization of pH	32
3.10	Dosage Optimization	33
3.11	Optimization of Rhodamine B (RhB) Dye Concentration.	33
3.12	Temperature Optimization at Room Temperature and 50 ^{0}C	34
3.13	Langmuir Isotherm Plot	35

3.14	Freundlich Isotherm Plot	36
3.15	Temkin Isotherm Plot	37
3.16	Pseudo First Order Kinetic Model	38
3.17	Pseudo Second Order Kinetic Model	39
3.18	Elovich Model	40

List of Tables

Serial No.	Title	Page No.
3.1	Average crystallite size	25
3.2	Isotherm parameters of RhB dye adsorption onto ZnO-CuO NPs.	37
3.3	Kinetic parameters of RhB dye adsorption onto ZnO-CuO NPs.	41

Nomenclature

Abbreviation	Full Form
ZnO	Zinc Oxide
CuO	Copper Oxide
$ZnCl_2$	Zinc Chloride
$CuCl_2$	Cupric Chloride
NH_4OH	Ammonium Hydroxide
HCl	Hydrochloric acid
RhB	Rhodamine B dye
CNTs	Carbon nanotubes
MWNTs	Multi-Walled Carbon nanotubes
SWNTs	Single-Walled Carbon nanotubes
XRD	X-Ray diffraction
FT-IR	Fourier Transform Infrared Spectroscopy
SEM	Scanning Electron Microscopy
UV-DRS	UV-Visible Diffuse Reflectance Spectroscopy
TGA	Thermogravimetric Analysis
BET	Brunauer–Emmett–Teller

Contents

Serial No.	Title	Page No.
	Chapter 1	
	Introduction	
1.1	**Introduction**	4
1.2	**What is Nanomaterial?**	4-5
1.3	**Classification of nanomaterials**	5-8
1.3.1	Carbon based nanoparticles	5
1.3.2	Metal Nanoparticles	6
1.3.3	Metal Oxide Nanoparticles	7
1.3.4	Ceramic Nanoparticles	7
1.3.5	Semiconductor nanoparticles	7
1.3.6	Polymeric Nanoparticles	7-8
1.4	**Synthesis of Nanoparticles**	8-9
1.4.1	Physical Methods	9
1.4.2	Chemical Methods	9
1.4.3	Biological Methods	9
1.5	**Water pollution**	10
1.6	**Sources of Water pollution**	10-11
1.7	**Techniques for Water Decontamination**	11-12
1.7.1	Physical methods	11
1.7.2	Chemical methods	11-12
1.8	**Motivation for selecting ZnO-CuO nanocomposite**	12-13
1.9	**Aim and Objectives of the Study**	13
	Chapter 2	
	Experimental work	
2.1	**Chemicals Required**	15
2.2	**Synthesis of materials**	15-16
2.2.1	Preparation of plant extract	15
2.2.2	Synthesis of ZnO-CuO nanocomposite	15

2.3	**Characterization**	17
2.4	**Batch adsorption experiment**	17-18
2.5	**Adsorption isotherms**	18-20
2.6	**Adsorption kinetics**	20-21
	Chapter 3	
	Results and discussion	
3.1	**Characterization**	23-31
3.1.1	Powder X-Ray Diffraction Analysis (PXRD)	23
3.1.2	Fourier Transform Infrared Spectroscopy (FTIR) Analysis	25
3.1.3	Scanning Electron Microscopy (SEM) Analysis	27
3.1.4	UV-Diffusion Reflectance Spectroscopy	29
3.1.5	BET analysis	30
3.1.6	Thermogravimetric Analysis (TGA)	31
3.2	**Optimization of Adsorption Parameters for the Removal of Rhodamine B Dye using ZnO–CuO Nanocomposite**	31-34
3.2.1	pH optimization	32
3.2.2	Dosage optimization	32
3.2.3	Optimization of Rhodamine B (RhB) Dye concentration	33
3.2.4	Temperature Optimization	34
3.3	**Adsorption Isotherm Modelling**	34-37
3.3.1	Langmuir Isotherm	35
3.3.2	Freundlich Isotherm	35
3.3.3	Temkin Isotherm	36
3.4	**Adsorption Kinetics**	38-41
3.4.1	Pseudo-First Order Kinetics	38
3.4.2	Pseudo-Second Order Kinetics	39
3.4.3	Elovich Kinetic Model	40
	Chapter 4	
	Conclusions	
4.1	**Conclusions**	43-44

CHAPTER 1

INTRODUCTION

1.1. Introduction

Nanotechnology is a field that has steadily grown in importance over the last few decades. It focuses on working with extremely small-scale materials—typically between 1 and 100 nanometres. At this scale, matter behaves differently, which opens up new possibilities for scientific research and practical applications. The term "nano" comes from ancient Greek and Latin roots meaning "dwarf," which fits the concept well, given the minuscule size we're dealing with.

What makes nanotechnology stand out is its interdisciplinary nature. It blends physics, chemistry, biology, material science, and engineering concepts. Because of this, anyone working in the field needs more than just knowledge in one subject—they need to understand how these areas connect and interact at the nanoscale.

One of the core ideas in nanotechnology is that when materials are reduced to very small sizes, their properties often change unexpectedly. For instance, materials that are inert or weak in bulk form might become reactive or stronger at the nanoscale. This allows scientists to design new types of materials with enhanced or completely novel characteristics.

Although most people don't think about nanotechnology in their daily lives, it's already being used in many areas. You'll find it in medicine, electronics, environmental solutions, and even defence systems. Despite this, public awareness of how widespread and impactful nanotechnology is remains fairly low. As the field keeps advancing, it's likely to play an even bigger role in shaping the technologies we use every day.

It's also useful to separate the terms "nanoscience" and "nanotechnology." Nanoscience is more about understanding how materials behave at the nanoscale—how atoms are arranged, and how their properties change. Nanotechnology takes that knowledge and puts it to use, creating materials, tools, or systems that benefit from those unique small-scale behaviours[1].

1.2. What is a Nanomaterial?

Nanomaterials are defined as substances that have at least one dimension measuring less than 100 nanometers, making them significantly smaller than objects observable under a conventional microscope. To give perspective, a nanometer is one-billionth of

a meter (1×10^{-9} m). At this incredibly small scale, the physical and chemical behavior of materials begins to change in unique ways. Their physicochemical properties—such as melting point, solubility, and reactivity often differ greatly from those of the same material in bulk form. These variations arise mainly due to the increased surface area and quantum effects that dominate at the nanoscale [2].

The shape and size of nanomaterials are critical in determining their overall characteristics. By controlling these aspects, scientists can tailor materials with specialized functions and novel properties not found in their larger-scale counterparts. Nanomaterials can appear in various structural forms, often categorized by their dimensionality. For example, nanoparticles are considered zero-dimensional (0D) because all their dimensions are within the nanoscale. Nanorods and nanotubes, on the other hand, are one-dimensional (1D), as they are significantly longer in one direction. Two-dimensional (2D) nanomaterials include nanosheets or thin films, where two dimensions are larger than the third.

When these nanoscale components interact or cluster together, their collective properties can change once again. This leads to the formation of more complex three-dimensional (3D) nanostructures, sometimes referred to as bulk nanomaterials, where the interactions between particles can influence thermal, mechanical, or optical behaviour[3].

1.3. Classification of Nanomaterials

Nanomaterials are categorized into a number of classes based on their size, shape and chemical composition. Figure 1.1 depicted the classification of nanomaterials. Based on their physical and chemical characteristics, some of the most well-known classes of NPs are describes below.

1.3.1. Carbon Based Nanoparticles.

The two primary categories of carbon-based NPs are fullerenes and carbon nanotubes (CNTs).

A. Fullerenes.

Spherical carbon molecules known as fullerenes (C60) are composed of carbon atoms joined by sp^2 hybridization. About 28 to 1500 carbon atoms make up the spherical structure, and the diameters of single-layer fullerenes range from 8.2 nm to 4-36 nm. Fullerenes contain nanomaterials made of globular hollow cages, including allotropic forms of carbon. Their great strength, structure, electron affinity, electrical conductivity, and versatility have drawn commercial interest[4].

B. Graphene

Graphene is an allotrope of carbon. Carbon atoms make up the two-dimensional planar hexagonal network of honeycomb lattices known as graphene. Typically, graphene sheets have a thickness of around 1 nm.

C. CNTs (carbon nanotubes).

Graphene nanosheets with a honeycomb structure can form carbon nanotubes (CNTs) when rolled into hollow coils. CNTs range from 0.7 nm for single-walled (SWNTs) to 100nm for multi-walled (MWNTs), with lengths from a few micrometers to millimeters. They can have one, two, or more walls. Recently, the chemical vapor deposition (CVD) technique has been used to create them.

B. Carbon Nanofibers.

Carbon nanofiber is made similarly to graphene nano foil and carbon nanotubes. The difference is that, instead of using standard cylindrical tubes, it is wrapped into a cone shape.

E. Black Carbon

The typical shape of an amorphous carbon material is spherical, with diameters between 20 and 70 nm. The particles interact quickly, causing them to aggregate and create agglomerates that are almost 500 nm in size[5].

1.3.2. Metal Nanoparticles.

Destructive or constructive methods are used to create metal-based nanoparticles from metals to nanometric sizes. There are synthesized nanoparticles of practically every metal. For the creation of nanoparticles, aluminium, cadmium, cobalt, copper, gold, iron, lead, silver, and zinc are frequently utilized. Sizes between 10 and 100 nm, surface features such as pore size, high surface to volume ratio, surface charge with density, crystalline structure, spherical forms, colour, reactivity, and sensitivity are some of the unique characteristics of nanoparticles. Metal NPs are synthesized using

metal precursors. These NPs exhibit special optoelectrical properties due to restricted surface plasmon resonance (SPR). The synthesis of size and shape-controlled metal nanoparticles is essential in today's advanced materials[6].

1.3.3. Metal Oxide Nanoparticles

Because of their special physical and chemical characteristics, like heat transfer and thermal conductivity, metal oxide nanoparticles are regarded as one of the most promising nanomaterials in many fields. Numerous metal oxide nanoparticles have been employed in the oil and gas sector for nearly every aspect of hydrocarbon E&P, including as a catalyst, wettability agent, enhanced oil recovery, reservoir imaging, filler or additive in drilling/completion fluid, and for trapping and fine particle mobility control. Among the various kinds of metal oxide nanoparticles, Fe_2O_3, SiO_2, Al_2O_3, MgO, ZrO_2, CeO_2, TiO_2, and ZnO are the most often utilized. Based on the type of phase change, metal oxide nanoparticle synthesis can generally be classified into two groups: liquid-solid and gas-solid.

1.3.4. Ceramic Nanoparticles

Heating and cooling are used to create ceramic NPs, which are non-metallic inorganic solids. They are amorphous, polycrystalline, dense, porous, and hollow, among other sizes and shapes. Researchers are paying close attention to these NPs because of their use in processes like catalysis, dye degradation, photo-catalysis, and imaging.

1.3.5. Semiconductor Nanoparticles

Semiconductor materials are used in a broad variety of literature because of their properties, which fall somewhere between those of metals and nonmetals. Bandgap tuning led to notable changes in the characteristics of semiconductor nanoparticles because of their enormous bandgaps. They are essential in electronic devices, photocatalysis, and optics. Several semiconductor nanoparticles are especially effective in water splitting applications because of their ideal bandgap and band edge positions.

1.3.6. Polymeric Nanoparticles

These are usually organic-based NPs, and they're referred to as polymer nanoparticles (PNPs) in the literature. Typically, they are nano-spherical or nano-capsular in form. The former are matrix particles with a solid overall mass, whereas the latter molecules are absorbed at the outside edge of the spherical surface. In the latter case, the solid mass is completely encapsulated within the particle. PNPs are simple to functionalize and, as a result, they have a wide range of uses in the literature. Lipid nanotechnology

is a specialized topic concerned with the design and manufacturing of lipid nanoparticles for several applications, such as medication delivery and RNA release in cancer[7].

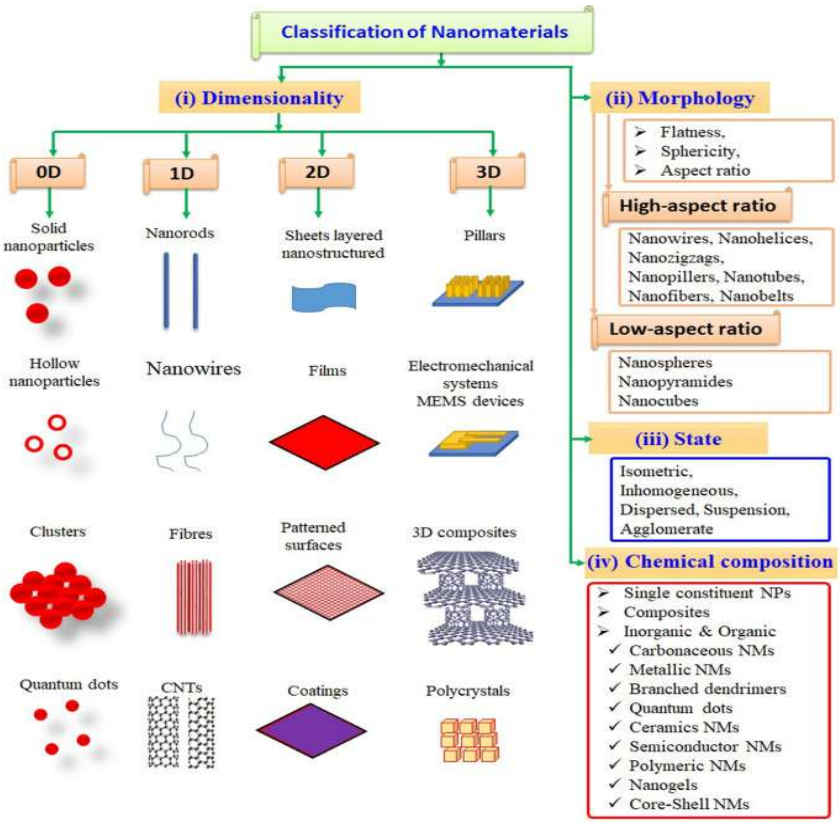

Figure 1.1. Classification of Nanomaterials

1.4. Synthesis of Nanoparticles

There are three different methods for synthesizing nanomaterials: physical, chemical, And biological methods as shown in Figure 1.2

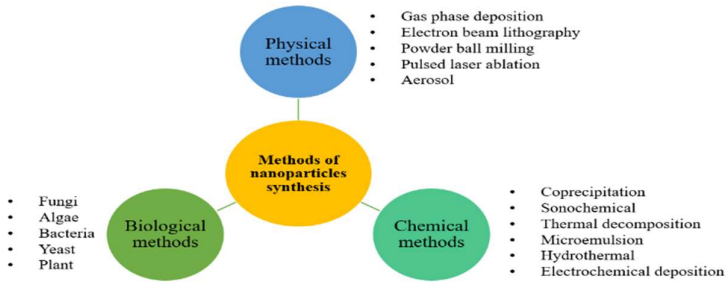

Figure 1.2. Schematic Illustration of the Several Procedures Used to Produce Nanoparticles

1.4.1. Physical Routes for the Synthesis of Nanoparticles

Nanomaterials are made *via* a variety of physical processes, including lithography, ball milling, gas-phase deposition, laser ablation, electrospinning, and sputtering. Target materials are vaporized by powerful laser beams during laser ablation, creating nanoparticles. Using focused light or electrons, lithography (both maskless and masked) produces nanopatterns; techniques like photolithography and nanoimprint lithography are frequently employed. One economical method of creating carbon nanoparticles and nanocomposites is by mechanical milling, particularly ball milling. A common method for creating polymer-based nano-fibers, including hybrid and core-shell architectures, is electrospinning.

1.4.2. Chemical Routes for the Synthesis of Nanoparticles

Nanomaterials are produced chemically by coprecipitation, microemulsion, hydrothermal, electrochemical deposition, and sono-chemical reactions. For high-quality graphene, chemical vapor deposition (CVD) is essential, whereas sol-gel is widely used for metal-oxide nanomaterials. Different nanostructures and homogeneous nanoparticles are produced by the soft template and reverse micelle techniques. To efficiently produce nanomaterials with various shapes, such as nanorods and nanosheets, microwave-assisted hydrothermal procedures are becoming more and more popular[8].

1.4.3. Biological Routes for Synthesis of Nanoparticles

Recently, a sustainable and eco-friendly substitute for conventional nanoparticle synthesis techniques is green synthesis. Conventional techniques sometimes include lengthy processes, hazardous chemicals and solvents, or waste products that can harm the environment and endanger the health of people and animals. The green synthesis approach, on the other hand, makes use of natural resources that are renewable and less harmful, like microbes and plant extracts, which may be restored over time. Furthermore, because these techniques are one-step syntheses that save energy and don’t require costly chemicals or equipment, they are frequently quicker and less expensive than conventional processes[9].

1.5. Water Pollution

The increasing pace of industrialization and civilization has made water contamination one of the most severe issues endangering the sustainability of the human species and

other life forms. Since the Industrial Revolution and human selfishness has caused dangerous contaminants to be released into water bodies, yet no attempt has been fully successful in stopping the behaviors that cause degradation in the environment. All living things are negatively impacted by these contaminants, which are dangerous and carcinogenic. Amazing attempts have therefore been made to use science and technology to obtain clean water[10].

1.6. Sources of Water Pollution

Textile industries are major sources of pollution in the environment, which cannot be removed by primary and secondary treatment. Water bodies are severely contaminated by the effluents from industries such as oil, refineries, and industrial facilities. Sewage discharge contains human waste, chemicals, and other pollutants also contaminate water bodies. Agricultural activities such as irrigation, pesticide and fertilizer used contribute to the contamination of water bodies (Figure 1.3).

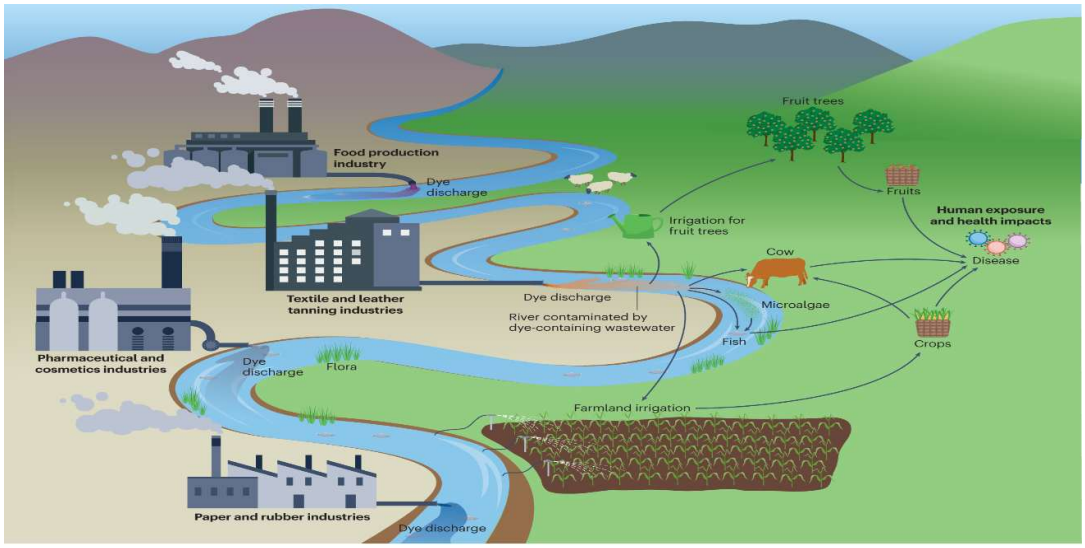

Figure 1.3. Source of water pollution

A range of organic compounds and heavy metals produced by chemical, oil refining, and steel sectors industries produce many harmful pollutants. Rainfall and atmospheric deposition can deposit pollutants into water sources, including acid rain and heavy metals. It's important to keep in mind that regulations, technological advancements, and better management practices may all contribute to reducing some of the causes of water pollution. However, reducing pollution from natural sources might be more challenging and require more innovative approaches[11].

1.7. Techniques Used for the Decontamination of Water

Various methods used for the decontamination of water are classified into physical methods and chemical methods.

1.7.1. Physical Methods

A. Sedimentation

The process of sedimentation involves letting suspended particles sink to the bottom of the water due to gravity. It's commonly used in wastewater treatment as well as in mining. There are three categories based on particle size: high concentration settling, flocculating particles, and constant settling. Shear forces, flow velocity, and particle size are some of the variables that affect efficiency.

B. Degasification

to enhance disinfection and stop corrosion, degasification eliminates dissolved gases from water, such as carbon dioxide, nitrogen, and oxygen. It releases gases mechanically using devices like membrane contactors, vacuum degassers, and air strippers.

C. Filtration

Filtration is the process of passing water through porous materials, such as gravel or sand, to eliminate contaminants. Membrane and particle filtration are two primary forms of filtration. Larger particles are filtered using bag filters, while smaller particles are filtered using a cartridge, which often has better filtration efficiency.

1.7.2. Chemical Methods

A. Disinfection

The method of disinfecting water involves adding chemicals such as ozone, chlorine, or chloramines to get rid of microorganisms.

B. Chemical precipitation

One method of treating water is chemical precipitation, which eliminates contaminants such as phosphorus, heavy metals, and suspended particles. The choice of coagulant, pH levels, mixing, and settling time are some of the variables that affect how effective the process is. It's frequently used in municipal water treatment and industrial settings.

C. Ion exchange

Ion exchange is a technique for treating wastewater that uses resin to replace unwanted ions with desired ones. It's frequently used in water softening and efficiently eliminates contaminants like heavy metals.

D. Adsorption

Adsorption is a successful method of purifying water in which impurities are drawn to and adhered to a porous adsorbent substance. The process can be divided into two categories: chemisorption and physisorption. In Chemisorption, chemical bonds are formed between the pollutant and the adsorbent, and in physisorption, pollutants bind due to weak van der Waals forces. Adsorption's ease of use and affordability make it a popular method for eliminating organic and natural contaminants from water. The contaminants are deposited on the surface of the adsorbent through intermolecular forces between the solid and liquid phases. Adsorbent dosage, surface area, pollutant concentration, temperature, pH, and contact time are some variables that affect adsorption efficiency. The ability to renew and reuse the adsorbent material is one of the primary benefits of this technique[12].

1.8. Motivation for Selection of Nanocomposites (ZnO-CuO)

The growing concern over water pollution caused by synthetic dyes released from textile, paper, and dyeing industries has prompted the need for effective and sustainable treatment methods. Among the various approaches, adsorption using nanomaterials has emerged as a highly efficient and practical technique due to its simplicity, cost-effectiveness, and high removal efficiency. In this context, the use of green-synthesized nanocomposites, particularly those involving metal oxides like ZnO and CuO, presents a promising solution. The motivation behind selecting bottle gourd (Lagenaria siceraria) extract and a ZnO-CuO nanocomposite for dye adsorption is rooted in both environmental sustainability and functional performance.

Bottle gourd is an underutilized but nutrient-rich plant, widely available and inexpensive, making it an ideal candidate for green synthesis. Its extract contains a rich mix of phytochemicals such as phenolics, flavonoids, and antioxidants, which act as natural reducing, stabilizing, and capping agents in the formation of nanoparticles. These compounds enable the synthesis of nanocomposites without the need for toxic or high-energy inputs. Using bottle gourd extract also supports eco-friendly processes, reduces chemical waste, and enhances the biocompatibility of the final product. Moreover, these bioactive compounds can contribute to the surface reactivity of the nanoparticles, potentially enhancing their adsorption capacity toward dye molecules.

The choice of ZnO and CuO is driven by their complementary structural and surface properties. ZnO offers a high surface area, porosity, and strong photocatalytic activity,

which can aid in the partial degradation of dye molecules in addition to adsorption. CuO adds enhanced surface affinity and catalytic behaviour, especially toward organic pollutants, due to its monoclinic structure and narrow bandgap. The combination of these two oxides in a ZnO-CuO heterojunction nanocomposite significantly improves surface reactivity, electron transport properties, and active sites available for dye binding. The synergistic interaction between ZnO and CuO promotes not only greater dye uptake but also improved recyclability and stability of the adsorbent material.

Additionally, the green synthesis route involving bottle gourd extract allows better control over the size, dispersion, and surface morphology of the nanocomposite, which directly influences adsorption efficiency. The presence of oxygen-containing functional groups from the plant extract further enhances the surface interaction with dye molecules through hydrogen bonding, electrostatic attraction, or π–π interactions, depending on the dye type[13].

In summary, the use of bottle gourd extract in the synthesis of ZnO-CuO nanocomposites represents a sustainable, low-cost, and effective approach for the removal of dye pollutants from wastewater. The integration of green synthesis with the functional advantages of ZnO and CuO not only aligns with environmental goals but also delivers a high-performance adsorbent material suitable for practical wastewater treatment applications.

1.9. Aim and Objectives of the Project

Aim:

- Green synthesis of ZnO-CuO nanocomposite for efficient adsorption of Rhodamine B dye

Objectives:

- Green synthesis of ZnO-CuO nanocomposite by using Lagenaria siceraria (Bottle gourd) peel extract.
- ZnO-CuO nanocomposite formation were confirmed by PXRD, IR whereas the morphological evidence was collected from SEM and BET Analysis.
- Application of Synthesized Nanocomposite for efficient adsorption of rhodamine B dye.

CHAPTER 2

EXPERIMENTAL WORK

2.1. Chemicals Required:

Zinc Chloride ($ZnCl_2$), Cupric Chloride ($CuCl_2$), deionized water, ethanol and Rhodamine-B were AR grade and procured from S-D fine chemicals. *Langenaria siceraria* (bottle gourd) was purchased from the vegetable market near VNIT, Nagpur.

2.2. Synthesis of Materials

2.2.1. Preparation of Plant Extract:

Fresh bottle gourd (*Lagenaria siceraria*) peels were collected, thoroughly rinsed under running tap water to remove surface impurities, and subsequently washed with distilled water to eliminate residual contaminants. The cleaned peels were then dried in the sunlight for approximately 3-5 days to remove moisture. Following drying, 10 grams of the dried bottle gourd peels were weighed using an analytical balance and then ground using the grinder to increase the surface area for extraction.

The 10g of dried peels were transferred into a 250 mL borosilicate glass beaker, to which 100 mL of distilled water was added. The mixture was subjected to gentle heating at 60°C for 30 minutes on a magnetic stirrer hotplate to facilitate the extraction of water-soluble phytoconstituents. Care was taken to avoid boiling, which could degrade heat-sensitive compounds.

After heating, the mixture was allowed to cool to room temperature. The resulting suspension was then filtered by using Whatman No. 1 filter paper to obtain a clear extract.

The filtrate (aqueous extract) was collected in a sterile glass bottle and stored at 4°C for further analysis.

2.2.2. Synthesis of ZnO-CuO Nanocomposite:

The green synthesis of zinc oxide–copper oxide (ZnO–CuO) nanocomposite was carried out using the aqueous extract of bottle gourd (*Lagenaria siceraria*) peels as a natural reducing and stabilizing agent. This environmentally friendly method offers a sustainable alternative to conventional chemical synthesis by avoiding the use of hazardous reagents and high-energy conditions.

Initially, freshly prepared bottle gourd peel extract, as described in Section 2.2.1, was used as the phytochemical source. The extract contains various bioactive compounds such as flavonoids, alkaloids, phenols, and saponins, which play a crucial role in reducing metal ions and stabilizing the nanoparticles.

To synthesize the nanocomposite, equimolar aqueous solutions, that is, 0.5M solutions of zinc chloride ($ZnCl_2$) and copper chloride ($CuCl_2$) were prepared separately by dissolving appropriate quantities in distilled water. 20 ml of $ZnCl_2$ solution was added dropwise to $CuCl_2$ solution. These metal precursor solutions were mixed under continuous stirring to ensure homogeneity. To this mixed metal salt solution, the bottle gourd extract was added dropwise while maintaining constant stirring for 1-2 hours.

During the reaction, a gradual colour change was observed, indicating the formation of ZnO–CuO nanocomposites. The mixture was allowed to cool naturally to room temperature, and the resulting precipitate was separated by centrifugation at 6,000 rpm for 15 minutes. The obtained solid was washed multiple times with distilled water and ethanol to remove any unreacted residues and phytochemicals.

The purified precipitate was then dried in a hot air oven at 80 °C for 5 hours. The dried powder was subsequently calcined in a muffle furnace at 400 °C for 6 hours to enhance the crystallinity and purity of the nanocomposite. Figure 2.1 depicted the systematic representation of the Synthesis of ZnO-CuO nanocomposite

This green synthesis approach is simple, cost-effective, and eco-friendly, making it suitable for scalable production and various biomedical and catalytic applications.

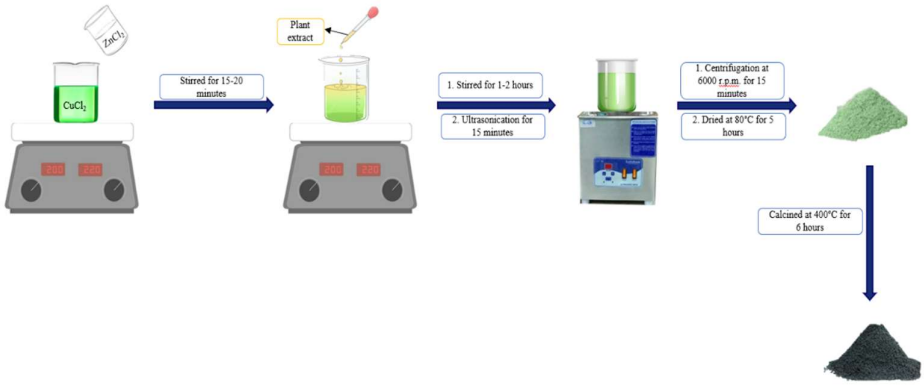
ZnCl2
CuCl2
Stirred for 15-20 minutes
Plant extract
1. Stirred for 1-2 hours
2. Ultrasonication for 15 minutes
1. Centrifugation at 6000 r.p.m. for 15 minutes
2. Dried at 80°C for 5 hours
Calcined at 400°C for 6 hours

Figure 2.1. Systematic Representation of the ZnO-CuO Nanocomposite Synthesis

2.3. Characterization

The synthesized ZnO–CuO nanocomposite was characterized using various analytical techniques to confirm its structure, morphology, and functional properties. Scanning Electron Microscopy (SEM) revealed nanoscale particles with irregular morphology and a tendency toward agglomeration, indicating successful synthesis. X-ray Diffraction (XRD) analysis confirmed the crystalline nature of the material, with distinct peaks corresponding to both ZnO and CuO phases, suggesting the formation of a mixed oxide composite. Fourier Transform Infrared Spectroscopy (FTIR) identified characteristic functional groups, as well as metal–oxygen bonds, confirming the presence of phytochemicals from the plant extract and successful metal oxide formation. Ultraviolet–Diffuse Reflectance Spectroscopy (UV–DRS) showed strong absorption in the UV region, and the estimated band gap energy suggested potential for photocatalytic applications. Additionally, Brunauer–Emmett–Teller (BET) surface area analysis indicated a mesoporous structure with a high specific surface area, making the nanocomposite suitable for surface-driven reactions such as adsorption and catalysis[14].

2.4. Batch Adsorption Experiment

The adsorption potential of Rhodamine B (RhB) dye onto ZnO–CuO nanocomposite synthesized using *Lagenaria siceraria* (bottle gourd) peel extract was examined through a series of controlled batch experiments. These studies were conducted in 100 mL of RhB dye solution with an initial concentration of 10 mg/L. A fixed amount (0.2 g) of the ZnO–CuO nanocomposite was added to the RhB solution, and the mixture was kept for stirring at a constant temperature of 25°C. Contact time intervals ranged from 15 minutes to 120 minutes to study the adsorption kinetics. At each selected interval, samples were withdrawn, centrifuged, and the residual RhB concentration was determined using a UV–Visible spectrophotometer at the dye's maximum absorbance wavelength (λmax).

To assess the effect of solution pH on adsorption efficiency, experiments were conducted across a pH range of 2 to 9. In each case, the pH was adjusted before adsorption using NH_4OH or HCl solutions. A constant adsorbent dose (0.2 g), dye concentration (10 mg/L), temperature (25°C), and agitation time (90 minutes) were maintained. The influence of initial dye concentration was also evaluated by varying RhB concentrations from 5 to 50 mg/L under the same conditions. Similarly, the effect of adsorbent dosage was assessed by

altering the amount of ZnO–CuO nanocomposite from 0.08 g to 0.2 g, using a fixed dye concentration of 10 ppm and an agitation time of 90 minutes. The influence of temperature on dye removal was analyzed by conducting adsorption trials at temperatures ranging from 25°C to 55°C, keeping other parameters constant.

The percentage removal of RhB dye (%R) was calculated using the following relation:

$$\%R = \frac{(C_i - C_f)}{C_i} \times 100$$

Where C_i- Initial Concentration and C_f- final concentrations of the dye (mg/L), respectively.

The equilibrium adsorption capacity (q_e) in mg/g was calculated using:

$$q_e = \frac{(C_i - C_f)V}{M}$$

Where V is the volume of the solution in litres, M is the weight of the adsorbent in grams[15].

2.5. Adsorption Isotherms

Adsorption isotherms are essential tools for understanding the nature and efficiency of adsorption processes, especially in the context of dye removal using nanomaterials. These isotherms illustrate the relationship between the quantity of adsorbate taken up by the adsorbent at equilibrium (q_e, in mg/g) and the equilibrium concentration of the adsorbate in the solution (C_e, in mg/L), all measured at a constant temperature. Analysing adsorption data using isotherm models allows for the estimation of adsorption capacity, surface characteristics, and the nature of the adsorbent–adsorbate interactions. In the present study, the equilibrium behaviour of Rhodamine B dye adsorption onto ZnO–CuO nanocomposite synthesized via green methods using *Lagenaria siceraria* (bottle gourd) extract was analysed using four widely recognized adsorption isotherm models: Langmuir, Freundlich, and Temkin.

The **Langmuir isotherm** is one of the most commonly used models for describing monolayer adsorption on a homogeneous surface, where all adsorption sites are assumed to be identical and energetically equivalent. The model also assumes that there is no lateral interaction between adsorbed molecules and that once a molecule occupies a site, no

further adsorption can occur at that site. It is suitable for representing chemisorption processes where strong adsorbent–adsorbate bonds form. The non-linear Langmuir equation is expressed as:

$$\frac{C_e}{q_e} = \frac{1}{q_{max} b} + \frac{C_e}{q_{max}}$$

Where q_{max} is the maximum monolayer adsorption capacity (mg/g), b is the Langmuir constant related to adsorption energy (L/mg), and C_e is the dye concentration at equilibrium. Additionally, the favourability of adsorption can be interpreted through the dimensionless separation factor R_L, given by:

$$R_L = \frac{1}{(1 + K_L C_0)}$$

where C_0 is the initial dye concentration. Values of R_L between 0 and 1 indicate favorable adsorption.

In contrast, the **Freundlich isotherm** accounts for heterogeneous surface energies, suggesting that different sites on the adsorbent have different affinities for the adsorbate. This model is empirical and supports multilayer adsorption with a non-uniform distribution of adsorption heat over the surface. The Freundlich equation is given by:

$$\log q_e = \log K_f + \frac{1}{n} \log C_e$$

where K_f and n are constants indicative of adsorption capacity and intensity, respectively. A value of 1/n less than 1 indicates favourable adsorption. This model is particularly applicable when dealing with complex natural adsorbents such as plant-based nanomaterials, where surface properties are inherently non-uniform.

The **Temkin isotherm** provides further insight into adsorbate–adsorbent interactions by incorporating the effect of indirect adsorbate/adsorbate interactions. It assumes that the heat of adsorption of all molecules decreases linearly with coverage due to these interactions. The Temkin model is expressed as:

$$q_e = B \ln K_t + B \ln C_e$$

where A_T is the Temkin equilibrium binding constant (L/g), and B is related to the heat of adsorption, calculated as $B = \frac{RT}{b}$ with R being the universal gas constant and T the absolute temperature. This model is more accurate for systems where the adsorption heat decreases gradually rather than abruptly with coverage.

By applying these isotherm models to the experimental data, one can not only estimate the adsorption efficiency but also determine which model best fits the behaviour of the system, thereby revealing the nature of the adsorption mechanism. Such analysis is crucial for designing practical adsorption systems for wastewater treatment using green-synthesized nanomaterials.

2.6. Adsorption Kinetics

Adsorption kinetics studies provide vital insight into the rate and mechanism by which adsorbate molecules interact with the surface of an adsorbent over time. Understanding these kinetics is essential in optimizing adsorption processes for practical applications such as wastewater treatment, where time-dependent adsorption behaviour influences the overall efficiency, design, and scale-up of treatment systems. In this study, the kinetic data for Rhodamine B dye adsorption onto green-synthesized ZnO–CuO nanocomposites were analysed using four different kinetic models: pseudo-first-order, pseudo-second-order, Elovich, and general-order kinetics.

The pseudo-first-order kinetic model, originally proposed by Lagergren, assumes that the rate of adsorption is directly proportional to the number of available active sites on the adsorbent surface, with the rate equation expressed as:

$$\ln(q_e - q_t) = \ln(k_1 q_e) - k_1 t$$

where qt and qe are the adsorption capacities at time t and equilibrium, respectively, and k_1 is the first-order rate constant. Conversely, the pseudo-second-order model assumes chemisorption is the rate-limiting step, involving valency forces through electron sharing or exchange between adsorbent and adsorbate. It is represented as:

$$\frac{t}{q_t} = \frac{1}{k_2 q_e^2} + \frac{t}{q_e}$$

Here, k_2 represents the rate constant for the pseudo-second-order kinetic model. The Elovich model, which is frequently used to characterize chemisorption on surfaces with a high degree of heterogeneity, proposes that the adsorption rate decreases exponentially as the surface becomes more saturated with adsorbate molecules. This model is mathematically expressed as:

$$q_t = \frac{1}{\alpha}\ln(\alpha\beta) + \frac{1}{\alpha}\ln t$$

In the Elovich model, the parameter α represents the initial rate at which adsorption occurs, while β corresponds to factors such as surface coverage and the activation energy required for the process[16].

CHAPTER 3

RESULTS AND DISSCUSION

3.1. Characterization

3.1.1. Powder X-Ray Diffraction Analysis (PXRD)

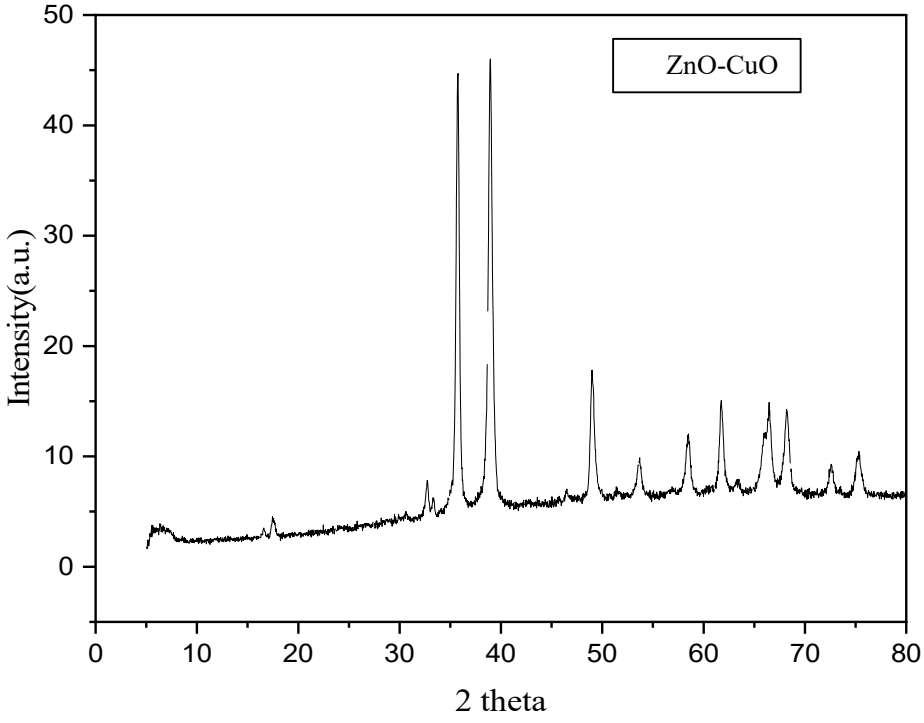

Figure 3.1. PXRD of ZnO-CuO nanocomposite.

The phase composition and crystalline features of the synthesized ZnO–CuO nanocomposite were examined using X-ray diffraction (XRD) analysis. The obtained diffractogram displayed characteristic peaks attributable to both ZnO and CuO, confirming the formation of a mixed-phase nanocomposite. Peaks corresponding to ZnO were identified at 2θ values of 31.76°, 34.4°, 36.28°, 47.58°, 56.62°, 62.84°, 66.36°, 67.98°, and 69.14° respectively. These reflections are consistent with the hexagonal wurtzite structure of ZnO, as per JCPDS card no. 00-036-1451. Additionally, the pattern revealed distinct peaks at 35.54°, 38.72°, 48.74°, 53.42°, 58.33°, and 61.6°, corresponding to the monoclinic CuO, which match the standard JCPDS card no. 00-048-1548. The simultaneous appearance of diffraction peaks for both metal oxides affirm the successful synthesis of a ZnO–CuO heterojunction nanocomposite. Furthermore, the absence of unindexed or unidentified peaks suggests a high level of phase purity, which is advantageous for applications like photocatalysis,

where structural integrity directly impacts charge transfer efficiency and catalytic performance.

To assess the nanocrystalline characteristics of the synthesized materials, the crystallite size was estimated using the Scherrer formula:

$$D = \frac{K\lambda}{\beta \cos \Theta}$$

In this equation:

D represents the average crystallite size,

λ represents the wavelength of the X-ray used, which is 1.5406 Å for copper K-alpha (Cu Kα) radiation.,

β refers to the full width at half maximum (FWHM), measured in radians.

θ is the Bragg diffraction angle.

Based on these measurements, the average crystallite size for the nanocomposite was found to be approximately 15.85 nm, confirming the successful formation of nanoscale crystalline domains.

Table 3.1. Average Crystallite Size

Peak Position(2θ)	FWHM	Crystallite size D (nm)	Average Crystallite size D (nm)
32.72	0.3948	20.97	**15.86**
35.74	0.4052	20.60	
38.96	0.5262	16.01	
49.03	0.4646	18.79	
53.65	0.4018	22.16	
64.97	64.808	0.1453	
66.30	0.9156	10.36	
68.21	0.5386	17.81	

The significance of these nanoscale crystallite sizes lies in their direct impact on the performance of the materials. Nanocrystals offer a higher surface area-to-volume ratio, which not only provides more active sites for surface reactions but also facilitates the efficient adsorption of dye[17].

3.1.2. Fourier Transform Infrared Spectroscopy (FTIR)

Fourier-transform infrared (FTIR) spectroscopy was employed to investigate the functional groups involved in the green synthesis of the ZnO–CuO nanocomposite and to confirm the presence of characteristic metal–oxygen bonds. The analysis was carried out over the spectral range of 400 to 4000 cm^{-1}, providing detailed insight into both the organic constituents from the plant extract and the metal oxide framework of the synthesised material.

The FTIR spectrum (figure 3.2) of the green-synthesised ZnO–CuO nanocomposite displayed several prominent absorption bands indicative of both the phytochemicals derived from the plant extract and the metal–oxygen bonding structure of the final nanocomposite. A strong and broad absorption band was observed in the region of 3200–3600 cm^{-1}, which can be attributed to O–H stretching vibrations. This broad peak is typically associated with hydroxyl groups present in polyphenols, flavonoids, or alcohols from the plant extract, as well as moisture adsorbed on the surface of the nanoparticles. Such phytochemicals act as both reducing and stabilising agents during the green synthesis process. In the region around 1600–1650 cm^{-1}, a distinct band was observed, corresponding to C=O stretching vibrations, often present in carboxylic acids or amide groups.

Most importantly, characteristic peaks in the low-frequency region between 400 and 600 cm^{-1} were observed, which are indicative of metal–oxygen bonding. The peak around 520–540 cm^{-1} corresponds to the stretching vibration of Cu–O bonds, while the band near 570–590 cm^{-1} is attributed to Zn–O stretching modes. These distinct vibrational features confirm the successful formation of ZnO and CuO phases in the synthesised nanocomposite.

The presence of bio-functional groups on the surface of the nanocomposite not only validates the role of plant metabolites in the synthesis process but may also enhance the surface reactivity of the material. These residual organic moieties can potentially influence photocatalytic or antimicrobial activity by interacting with external species through hydrogen bonding or redox reactions.

In summary, FTIR spectroscopy confirmed the successful synthesis of the ZnO–CuO nanocomposite via a green route using plant extract. The identified bands illustrate the presence of metal–oxygen bonds essential for oxide formation and suggest effective participation of plant-derived compounds in nanoparticle synthesis. These findings provide valuable insight into the eco-friendly nature of the synthetic pathway and highlight the multifunctional role of phytochemicals as reducing, capping, and stabilizing agents[18].

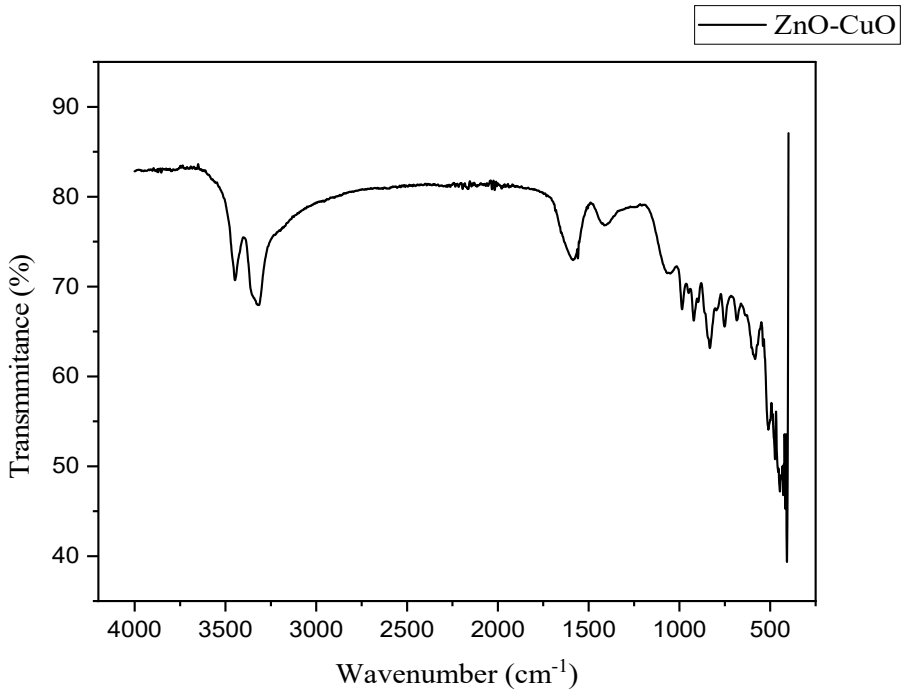

Figure 3.2. FTIR analysis on ZnO-CuO.

3.1.3. Scanning Electron Microscopy (SEM) Analysis

Figure 3.3. (a), (b) and (c) SEM images of ZnO-CuO nanocomposite

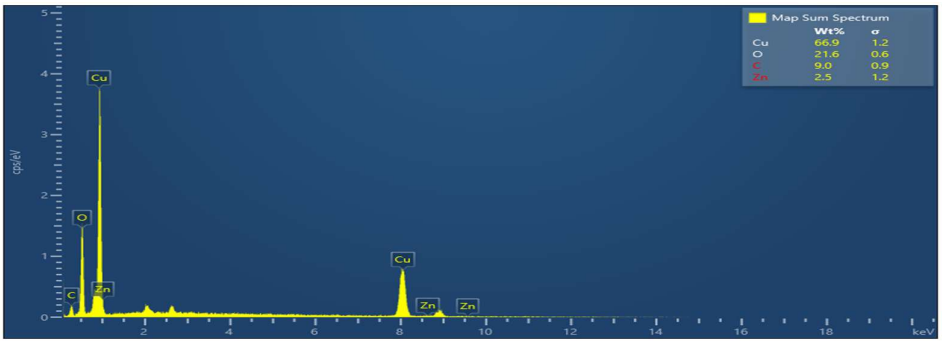

Figure 3.4. EDX Analysis.

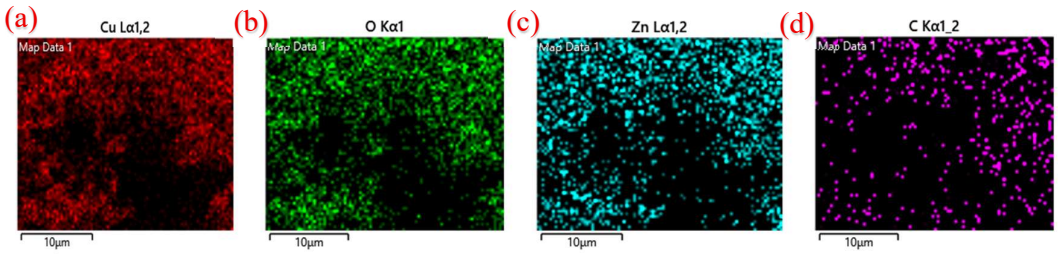

Figure 3.5. (a),(b) and (c) Elemental mapping of ZnO-CuO nanocomposite.

The surface morphology of the synthesised ZnO–CuO nanocomposite was investigated through Scanning Electron Microscopy (SEM). The micrographs revealed that the surface of the composite was composed of irregularly distributed nanostructures, as shown in Figure 3.3. Specifically, ZnO appeared predominantly in elongated rod-like shapes, whereas CuO was identified as fine granular or nearly spherical particles. Notable agglomeration was observed in various regions of the material, which can be attributed to the intrinsic high surface energy of nanoparticles.

To verify the elemental composition of the nanocomposite, Energy Dispersive X-ray Spectroscopy (EDX) was employed. The resulting spectra displayed distinct signals corresponding to zinc (Zn), copper (Cu), and oxygen (O), confirming the successful formation of a bimetallic oxide system as shown in Figure 3.4. Additionally, a carbon (C) peak was identified. This is commonly associated with the minor residues or remnants from phytochemical compounds. No additional peaks corresponding to foreign elements were observed, supporting the elemental purity of the synthesised composite.

Elemental mapping was performed to evaluate the spatial distribution of the main constituents—Zn, Cu, O, and C within the nanocomposite matrix. The distribution maps demonstrated a relatively even dispersion of all three elements across the observed field as shown in Figure 3.5. However, zones with higher intensity signals coincided with areas where nanoparticle aggregation had taken place. These findings suggest that despite the clustering of some particles, both ZnO and CuO phases were uniformly integrated throughout the composite, thereby facilitating efficient interfacial contact. The carbon signal, as expected, appeared sparsely and irregularly in the background, reinforcing the assumption that it originated from phytochemical compounds[19].

3.1.4. UV-Diffusion Reflectance Spectroscopy:

UV–Vis Diffuse Reflectance Spectroscopy (UV–DRS) was employed to study the optical properties of the ZnO–CuO nanocomposite. This method is particularly useful for analysing powders and opaque materials, where traditional transmission techniques are not feasible. In this technique, incident light in the ultraviolet and visible range is scattered upon contact with the sample surface, and the reflected light is collected to assess the material's absorption characteristics.

The data obtained through UV–DRS (figure 3.6) allows for the evaluation of the material's optical absorption near the fundamental absorption edge, which is closely related to the electronic structure of the sample. By analysing how the nanocomposite interacts with light, insights into electronic transitions and energy levels can be obtained. This is particularly important for semiconductors, where the energy band gap determines their suitability for various applications, including photocatalysis and environmental remediation.

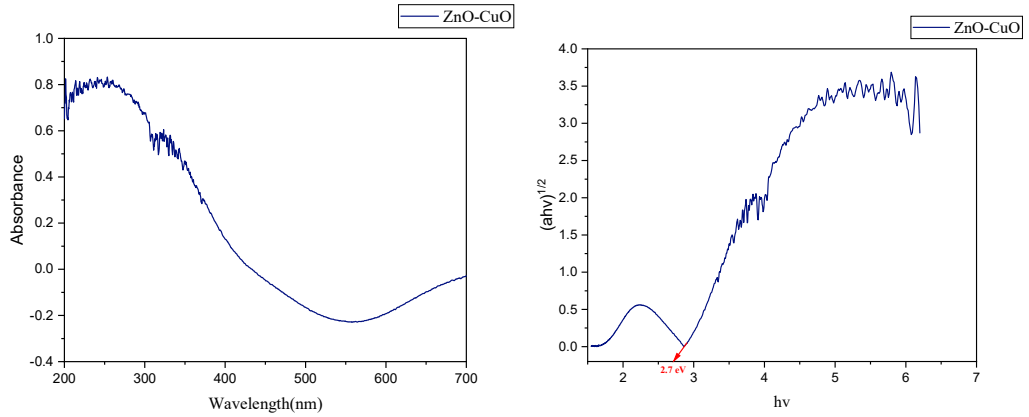

Figure 3.6. a) UV-DRS spectra and b) Tauc plot.

In the present study, the optical band gap of the ZnO–CuO nanocomposite was estimated to be approximately 2.7 eV. This value indicates the material's capability to absorb light in the visible spectrum, enhancing its effectiveness for photocatalytic and adsorptive applications. The observed band gap is slightly lower than that of pure ZnO, suggesting that the combination of ZnO and CuO in the nanocomposite has led to the formation of new energy states or structural changes that contribute to this narrowing.

Such a reduction in the band gap can be beneficial in environmental technologies, particularly in the degradation of organic pollutants under visible light. The interaction between ZnO and CuO phases likely facilitates charge separation and reduces recombination of electron–hole pairs, which further supports enhanced performance in photocatalytic and adsorption processes[20].

3.1.5. BET Analysis:

The Brunauer–Emmett–Teller (BET) technique was employed to determine the specific surface area and porosity of the green-synthesized ZnO–CuO nanocomposite. Nitrogen adsorption–desorption measurements were conducted at to assess the material's textural characteristics, which are essential for applications in adsorption and photocatalysis.

The nanocomposite exhibited a BET surface area of 11.541 m^2/g, indicating a moderately active surface capable of facilitating surface interactions with target pollutants.

The average pore radius was calculated to be approximately 2.20 nm, placing it within the mesoporous range (2–50 nm), which is favourable for the diffusion and retention of dye molecules and other organic compounds. The mesoporosity of the material supports enhanced adsorption performance and efficient light-induced catalytic reactions by providing more active sites and facilitating mass transport.

These textural features, particularly the moderate surface area and mesopore size distribution, contribute to the effectiveness of the ZnO–CuO nanocomposite in environmental remediation processes[21].

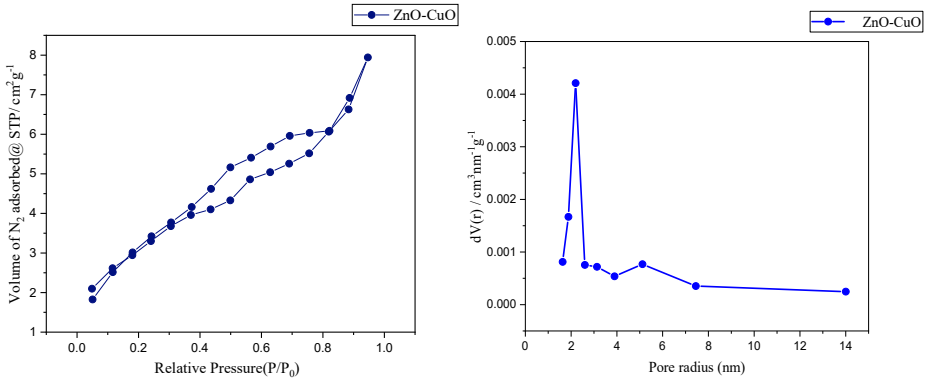

Figure 3.7. (a)N_2 adsorption-desorption isotherm and (b) pore size distribution of ZnO-CuO

3.1.6. Thermogravimetric Analysis (TGA)

Thermogravimetric Analysis (TGA) was carried out to evaluate the thermal stability and decomposition behavior of the ZnO–CuO nanocomposite. Figure 3.8 represents the thermogravimetric analysis for synthesised ZnO–CuO nanocomposite. The analysis was performed in an air atmosphere, with the sample heated from room temperature up to 800 °C at a constant heating rate[22].

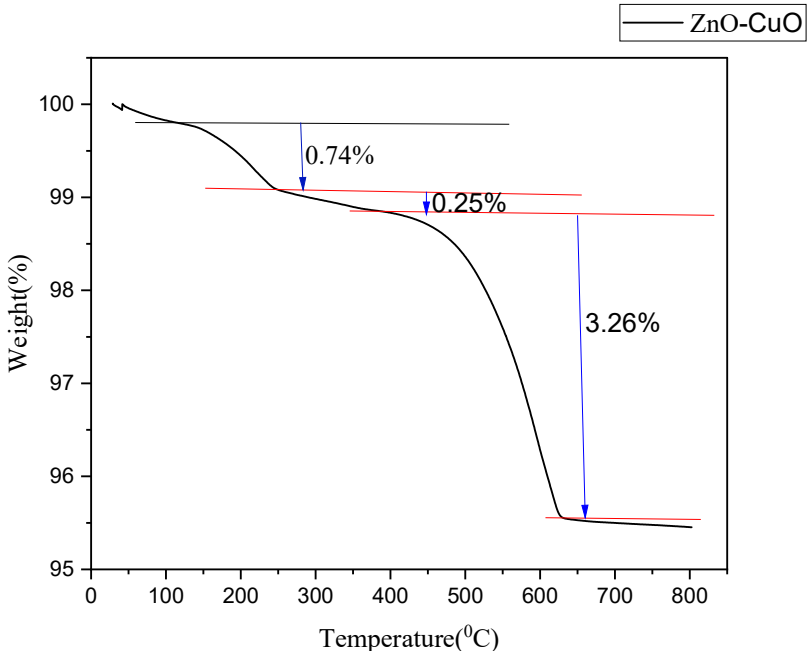

Figure 3.8. Thermogravimetric analysis

The TGA analysis confirmed the successful formation of a stable binary oxide system, with minimal organic contamination and good thermal resistance, reinforcing the potential of the nanocomposite for industrial and environmental applications.

3.2. Optimization of Adsorption Parameters for the Removal of Rhodamine B Dye using ZnO–CuO Nanocomposite

To optimize the adsorption of Rhodamine B (RhB) dye using the synthesized ZnO–CuO nanocomposite, a series of experiments were conducted, focusing on the influence of various parameters such as pH, nanocomposite dosage, initial dye concentration, and temperature. For each optimization step, 200 mg of the ZnO–CuO nanocomposite was

added to 100 mL of a 10 ppm RhB solution. For analysis UV-Visible spectroscopy (UV-1800) Shimadzu was used.

3.2.1. pH Optimization

The pH of the dye solution was adjusted using either hydrochloric acid (HCl) or ammonium hydroxide (NH_4OH), covering a range from acidic to alkaline conditions (typically between pH 3 and pH 9). It was hypothesized that the pH of the solution would significantly affect the surface charge of the nanocomposite and the ionization of the dye molecules, thereby influencing the adsorption efficiency. The optimization of pH was performed by measuring the percentage removal of RhB at each pH value to identify the pH at which maximum dye removal occurred.

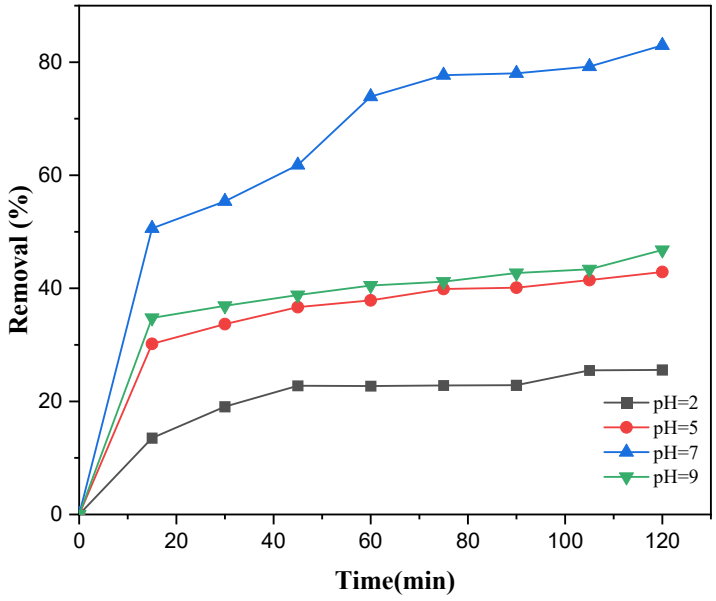

Figure 3.9. Optimization of pH

3.2.2. Dosage Optimization

The dosage of the ZnO–CuO nanocomposite was varied to assess its effect on the adsorption capacity. A range of dosages, typically between 80 mg and 200 mg per 100 mL of solution, was tested. It was expected that increasing the dosage would increase the number of available adsorption sites, leading to higher dye removal.

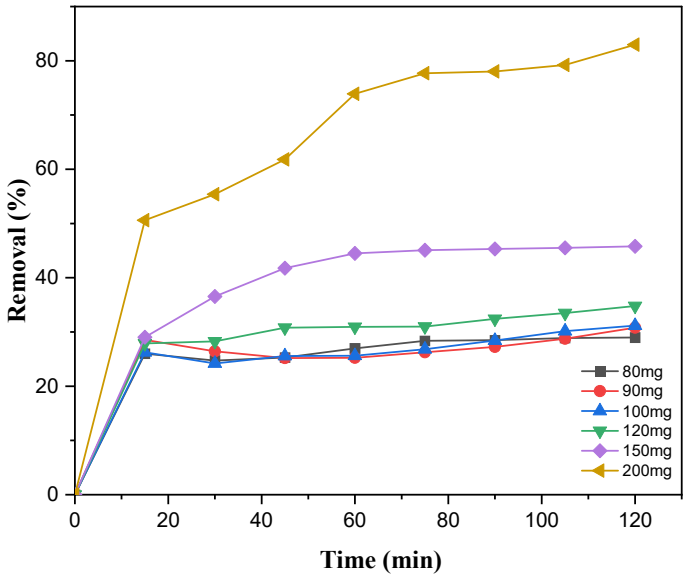

Figure 3.10. Dosage Optimization

3.2.3. Optimization of Rhodamine B (RhB) Dye Concentration

The effect of initial dye concentration was also studied by conducting adsorption experiments at various concentrations, such as 5 ppm, 10 ppm, 20ppm and 30 ppm. This step was crucial in understanding how the initial dye concentration influences the adsorption process, as higher concentrations might lead to saturation of adsorption sites and reduced removal efficiency.

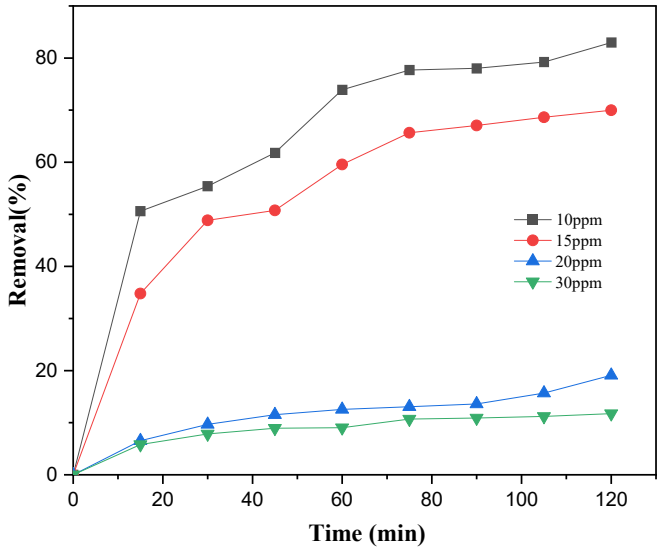

Figure 3.11. Optimization of Rhodamine B (RhB) Dye Concentration.

3.2.4. Temperature Optimization

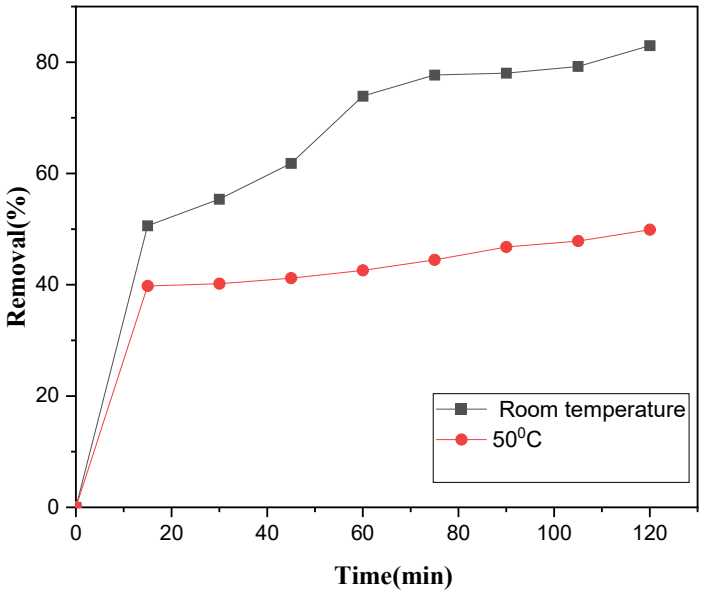

Figure 3.12. Temperature Optimization at Room Temperature and 50^{0}C

Temperature plays a crucial role in determining the efficiency of adsorption processes. In this study, temperature optimization was carried out to examine its effect on the removal of Rhodamine B (RhB) dye using ZnO–CuO nanocomposites synthesized through a green method employing bottle gourd peel extract. The experiments were performed at two different temperatures: room temperature (approximately 25 °C) and 50 °C. The results showed that the adsorption capacity was higher at room temperature compared to 50 °C, indicating that lower temperatures favour the adsorption of RhB onto the ZnO–CuO surface. This suggests that the adsorption process is exothermic in nature. These findings highlight that ambient conditions are more suitable for efficient dye removal, making the process more energy-efficient and environmentally friendly.

3.3. Adsorption Isotherm Study

The adsorption behaviour of Rhodamine B (RhB) dye on the synthesized ZnO–CuO nanocomposite was evaluated by applying three classical isotherm models in their linearized forms: Langmuir, Freundlich, and Temkin. These models help to understand the nature of the adsorption process, such as surface characteristics, adsorption mechanism, and interaction strength between the adsorbate and adsorbent.

3.3.1. Langmuir Isotherm

The Langmuir model assumes monolayer adsorption on a surface with a finite number of uniform sites. The linear form of the Langmuir equation is:

$$\frac{C_e}{q_e} = \frac{1}{q_{max}b} + \frac{C_e}{q_{max}}$$

A plot of C_e/q_e versus C_e yielded a straight line (Figure 3.13), from which the maximum adsorption capacity (q_{max}) and the Langmuir constant (b) were determined.

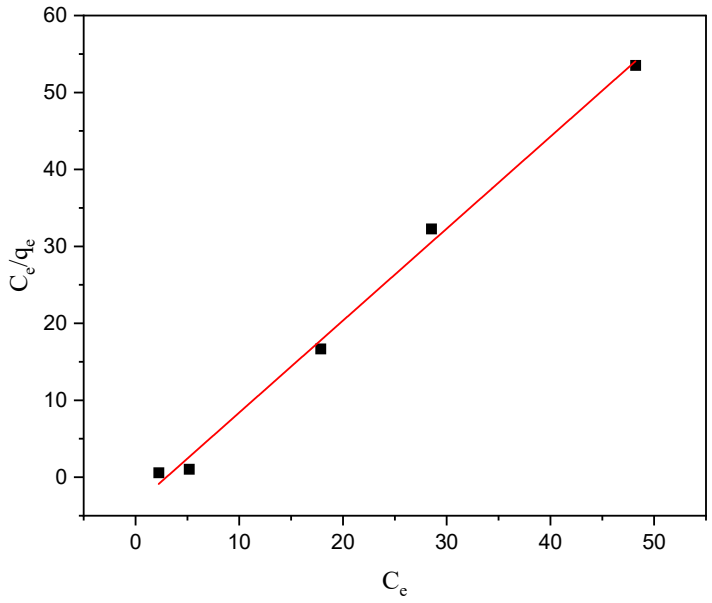

Figure 3.13. Langmuir Isotherm Plot

The high correlation coefficient ($R^2 = 0.99554$) confirms that the Langmuir model provides an excellent fit to the experimental data. This indicates that RhB molecules are adsorbed uniformly on the surface of the ZnO–CuO nanocomposite, suggesting a monolayer coverage and homogeneous adsorption sites.

3.3.2. Freundlich Isotherm

The Freundlich isotherm describes adsorption on a heterogeneous surface and allows for multilayer adsorption. The linear form is expressed as:

$$\log q_e = \log K_f + \frac{1}{n}\log C_e$$

The plot of log q_e versus log C_e showed relatively low linearity (figure 3.14), with a correlation coefficient of $R^2 = 0.46776$.

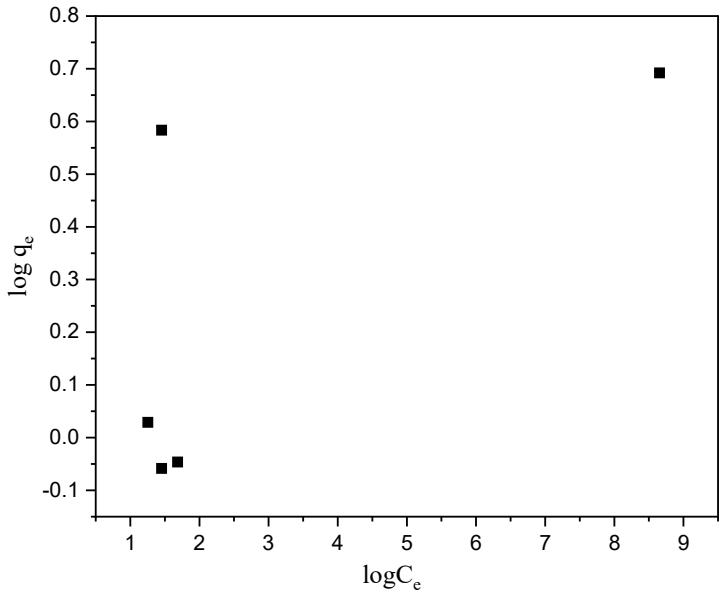

Figure 3.14. Freundlich Isotherm Plot

This weak correlation suggests that the Freundlich model is not well-suited for describing the adsorption of RhB on the ZnO–CuO nanocomposite. The result implies that the surface does not exhibit significant heterogeneity for this particular adsorbate, or that monolayer adsorption dominates over multilayer mechanisms.

3.3.3. Temkin Isotherm

The Temkin model considers adsorbent–adsorbate interactions and assumes that the heat of adsorption decreases linearly with increasing coverage. Its linear form is:

$$q_e = B \ln K_t + B \ln C_e$$

Here, A_T is the equilibrium binding constant, and B is related to the heat of adsorption.

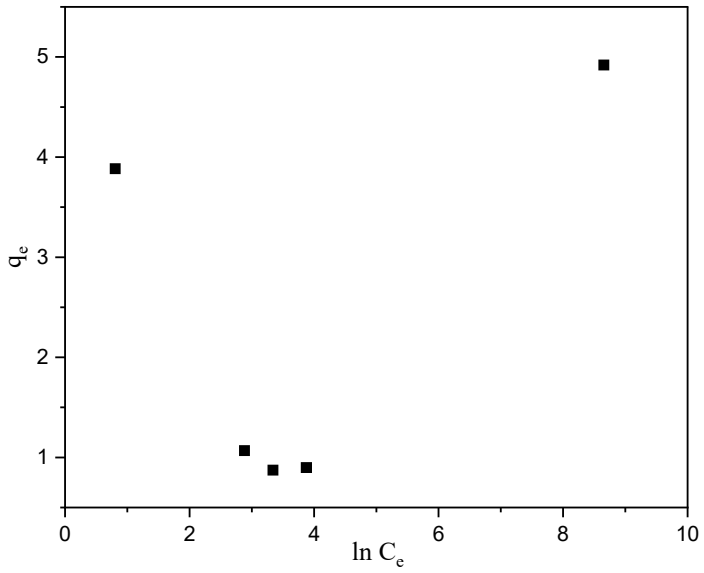

Figure 3.15. Temkin Isotherm Plot

The plot of q_e versus ln C_e (figure 3.15) produced a low correlation coefficient of R^2 =0.18562, indicating poor applicability of the Temkin model in this system. The weak fit suggests that RhB adsorption on the ZnO–CuO composite is not significantly influenced by variations in adsorption energy with coverage**.**

Table 3.2. Isotherm Parameters of RhB Dye Adsorption Onto ZnO-CuO NPs.

Isotherm Equations	Parameters	Value
Langmuir $\frac{C_e}{q_e} = \frac{1}{q_{max}b} + \frac{C_e}{q_{max}}$	q_e (mg/g)	0.8667
	K_L (L/mg)	0.7001
	R_L	0.1249
	R^2	0.9955
Freundlich $\log q_e = \log K_f + \frac{1}{n}\log C_e$	1/n	0.0779
	n	12.8436
	K_f	1.03445
	R^2	0.4678
Temkin $q_e = B \ln K_t + B \ln C_e$	A_T	67.2834
	B	0.2869
	R^2	0.1856

3.4. Adsorption Kinetics

Understanding the adsorption kinetics is essential for interpreting the mechanisms and dynamics of contaminant removal from aqueous solutions using nanomaterials. In this study, the kinetics of Rhodamine B (RhB) dye adsorption onto ZnO–CuO nanocomposites were evaluated using the pseudo-first-order, pseudo-second-order, and Elovich kinetic models. The models were applied in their linear forms, and the corresponding kinetic parameters were determined through linear regression.

3.4.1. Pseudo-First-Order Kinetic Model

The pseudo-first-order model assumes that the rate of adsorption is directly proportional to the number of unoccupied sites. The linear form of the model is expressed as:

$$\ln(q_e - q_t) = \ln(k_1 q_e) - k_1 t$$

Where:

- q_e is the equilibrium adsorption capacity (mg/g),
- q_t is the adsorption capacity at time t,
- k_1 is the pseudo-first-order rate constant (min^{-1}).

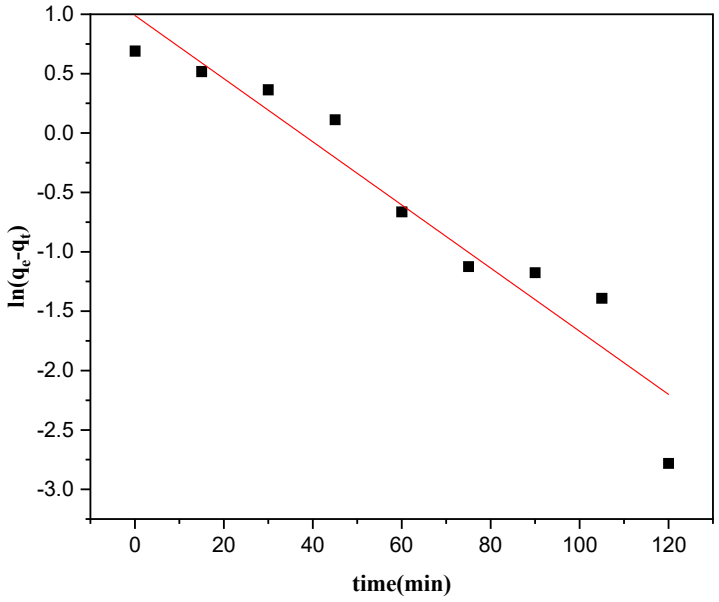

Figure 3.16. Pseudo-First-Order Kinetic Model.

For RhB dye adsorption, the model provided a correlation coefficient (R^2) of 0.92242, indicating a moderate fit. Although it suggests that physical adsorption could be a contributing mechanism, the deviation between experimental and calculated q_e values implies that this model alone does not adequately describe the system.

3.4.2. Pseudo-Second-Order Kinetic Model

The pseudo-second-order model presumes that the adsorption process is based on chemisorption, involving valence forces through the sharing or exchange of electrons. Its linearized equation is:

$$\frac{t}{q_t} = \frac{1}{k_2 q_e^2} + \frac{t}{q_e}$$

Where K_2 is the pseudo-second-order rate constant (g/mg·min).

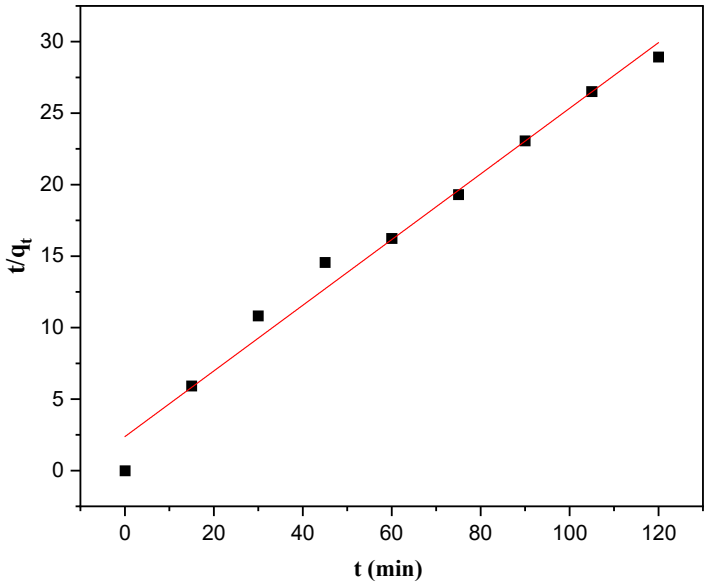

Figure 3.17. Pseudo-Second Order Kinetic Model.

This model showed the highest R^2 value of 0.98255, indicating an excellent agreement with the experimental data. The calculated q_e values closely matched the experimental results, reinforcing the inference that **chemisorption** is the predominant mechanism in RhB dye adsorption onto the ZnO–CuO composite.

3.4.3. Elovich Kinetic Model

The Elovich model is particularly effective for describing chemisorption on highly heterogeneous surfaces. Its linear form is:

$$q_t = \frac{1}{\alpha}\ln(\alpha\beta) + \frac{1}{\alpha}\ln t$$

Where:

- α is the initial adsorption rate (mg/g·min),
- β is a desorption constant (g/mg), related to surface coverage and activation energy.

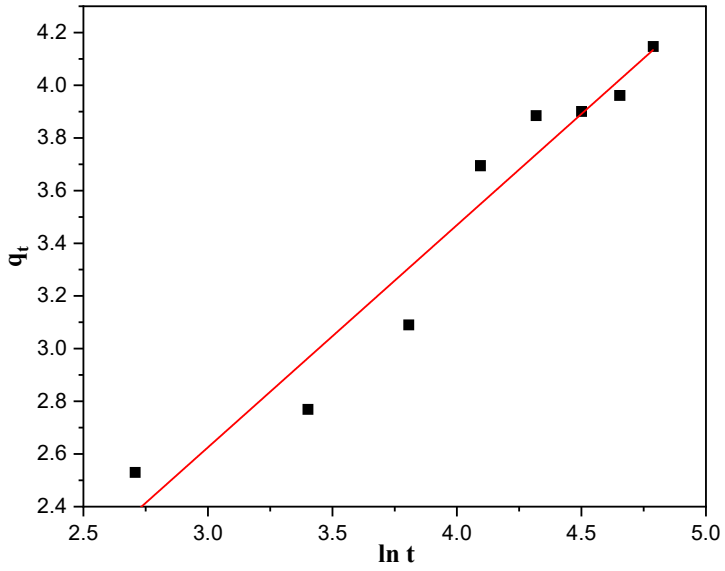

Figure 3.18. Elovich Kinetic Model

The Elovich model yielded an R^2 value of 0.94116, suggesting a fairly good fit and supporting the presence of heterogeneous adsorption sites. This aligns with the structural diversity observed in the SEM analysis, where ZnO and CuO particles form mixed morphologies, offering a variety of active sites for dye adsorption[13].

3.3. Kinetic Parameters of RhB Dye Adsorption onto ZnO-CuO NPs.

Kinetic Models	Parameters	Value
Pseudo first order $\ln(q_e - q_t) = \ln(k_1 q_e) - k_1 t$	q_e(mg/g) k_1 R^2	2.6916 -0.0002 0.9224
Pseudo second order $\frac{t}{q_t} = \frac{1}{k_2 q_e^2} + \frac{t}{q_e}$	q_e(mg/g) k_2 R^2	18.9612 0.0222 0.9825
Elovich $q_t = \frac{1}{\alpha}\ln(\alpha\beta) + \frac{1}{\alpha}\ln t$	α β R^2	1.1848 0.9424 0.9411

CHAPTER 4

CONCLUSIONS

4. Conclusions

This study successfully demonstrated the green synthesis of ZnO–CuO nanocomposites using bottle gourd (*Lagenaria siceraria*) peel extract as a bio-reductant and stabilizing agent. This environmentally friendly method offers a sustainable and low-cost alternative to traditional chemical synthesis, supporting the principles of green chemistry and waste utilization.

Comprehensive characterization techniques confirmed the formation and properties of the synthesized nanocomposite. X-ray diffraction (XRD) confirmed the presence of crystalline phases for both ZnO and CuO, indicating successful incorporation of the binary metal oxides. Fourier-transform infrared spectroscopy (FTIR) identified characteristic peaks of Zn–O and Cu–O bonds, along with signals related to plant-derived functional groups, supporting the involvement of phytochemicals in the reduction process.

UV-Vis diffuse reflectance spectroscopy (UV-DRS) analysis estimated the optical band gap of the nanocomposite to be approximately 2.7 eV, indicating its potential for visible light-driven applications. Thermogravimetric analysis (TGA) showed that the nanocomposite possesses good thermal stability, with observed weight losses corresponding to moisture release and decomposition of organic residues.

Scanning electron microscopy (SEM) revealed that the particles exhibited a mixed morphology, and significant aggregation was observed across the surface, which may be attributed to high surface energy and intermolecular interactions during the drying or synthesis process. Despite aggregation, the Energy Dispersive X-ray (EDX) analysis confirmed the elemental composition, with clear signals for Zn, Cu, and O, while elemental mapping showed a relatively uniform spatial distribution.

BET surface area analysis further supported the material's porosity, a beneficial trait for adsorption processes. The nanocomposite's performance was evaluated for the adsorption of Rhodamine B dye. Adsorption isotherms revealed that the Langmuir model provided the best fit ($R^2 = 0.99$), suggesting monolayer adsorption on a uniform surface. Kinetic studies showed that the adsorption followed a pseudo-second-order model ($R^2 = 0.98$), implying that chemisorption was the dominant mechanism.

Overall, the ZnO–CuO nanocomposite synthesized via a green route using bottle gourd peel extract demonstrated favourable structural and functional properties for environmental remediation applications. This approach highlights the viability of using agricultural waste for the eco-friendly development of multifunctional nanomaterials.

References

1. Nasrollahzadeh M., Sajadi S. M., Sajjadi M., & Issaabadi Z.(2019). An introduction to nanotechnology. *Interface Science and Technology. Vol 28*,1–27. https://doi.org/10.1016/B978-0-12-813586-0.00001-8
2. Yang, Chun Cheng, & Mai, Yiu-Wing. (2014). Thermodynamics at the nanoscale: A new approach to the investigation of unique physicochemical properties of nanomaterials. *Materials Science and Engineering: R: Reports, 79*, 1–40. https://doi.org/10.1016/j.mser.2014.02.001.
3. Stolarczyk J. K, Deak A., & Brougham D. F.(2016). Nanoparticle clusters: assembly and control over internal order, current capabilities, and future potential. *Adv* Mater. 28(27), 5400-5424. https://doi.org/10.1002/adma.201505350.
4. Arshad, S., Hussain, A., Noreen, S., Bibi, N., Tahir, M. B., Rehman, J. ur, Jabeen, M., Munawar, H. B., & Rahman, S. (2023). Structural, mechanical, electronic, and optical properties of MFe_2O_4 (M = Zn, Cu, Si) ferrites for electrochemical, photocatalytic, and optoelectronic applications. *Journal of Solid State Chemistry*, *330*(3), 124504. https://doi.org/10.1016/j.jssc.2023.124504
5. Zhang, Y., Petibone, D., Xu, Y., Mahmood, M., Karmakar, A., Casciano, D., Ali, S., & Biris, A. S. (2014). Toxicity and efficacy of carbon nanotubes and graphene: The utility of carbon-based nanoparticles in nanomedicine. *Critical Reviews in Toxicology*, *44*(3), 193–213. https://doi.org/10.3109/03602532.2014.883406
6. Huang, J., Lin, L., Sun, D., Chen, H., Yang, D., & Li, Q. (2015). Bio-inspired synthesis of metal nanomaterials and applications. *Chemical Society Reviews*, *44*(14), 5016–5030. https://doi.org/10.1039/C5CS00133A
7. Saleh, T. A. (2020). Nanomaterials: Classification, properties, and environmental toxicities. *Environmental Technology & Innovation*, *20*, 101067. https://doi.org/10.1016/j.eti.2020.101067
8. Baral, S. C., Sharma, P., Kumar, A., Thakur, M., Mahato, M., Ray, S., & Sharma, S. (2023). An introduction to metal oxides. In P. Sharma & S. C. Baral (Eds.), *Optical Properties of Metal Oxide Nanostructures* (pp. 1–34). Springer.
9. Iravani, S., Zolfaghari, B., Fadaei, R., & Varma, R. S. (2014). Synthesis of silver nanoparticles: Chemical, physical, and biological methods. *Research in*

Pharmaceutical Sciences, *9*(6), 385–406. https://doi.org/10.4103/1735-5362.141032

10. Sakamoto, M., Islam, M. S., Rahman, M. S., & Hossain, M. (2019). Water pollution and the textile industry in Bangladesh: Flawed corporate practices or restrictive opportunities? *Sustainability*, *11*(7), 1951. https://doi.org/10.3390/su11071951
11. Singh, M. R., & Gupta, A. (2016). Water pollution-sources, effects and control. *Centre for Biodiversity, Department of Botany, Nagaland University*, 1–16.
12. Fox, K. R. (2009). Water treatment and equipment decontamination techniques. *Journal of Contemporary Water Research and Education*, *129*(1), 5.
13. Abegunde, S. M., Adebayo, M. A., & Olasehinde, E. F. (2024). Green synthesis of ZnO nanoparticles and its application for methyl green dye adsorption. *Green Energy and Resources*, *2*(2), 100073. https://doi.org/10.1016/j.greenres.2024.100073
14. Mohammadi-Aloucheh, R., Sadeghi, A., Ghaffari, M., & Khajeh, M. (2018). Green synthesis of ZnO and ZnO/CuO nanocomposites in *Mentha longifolia* leaf extract: Characterization and their application as anti-bacterial agents. *Journal of Materials Science: Materials in Electronics*, *29*, 13596–13605. https://doi.org/10.1007/s10854-018-8833-0
15. Chakraborty, S., Bhattacharyya, K. G., & Saha, S. (2005). Adsorption study for the removal of a basic dye: Experimental and modeling. *Chemosphere*, *58*(8), 1079–1086. https://doi.org/10.1016/j.chemosphere.2004.09.017
16. Muthukumaran, C., Sivakumar, V. M., & Thirumarimurugan, M. (2016). Adsorption isotherms and kinetic studies of crystal violet dye removal from aqueous solution using surfactant modified magnetic nanoadsorbent. *Journal of the Taiwan Institute of Chemical Engineers*, *63*, 354–362. https://doi.org/10.1016/j.jtice.2016.03.016
17. Bekru, A. G., Mola, G. T., Abate, G., & Geberemariam, A. D. (2022). Green synthesis of a CuO–ZnO nanocomposite for efficient photodegradation of methylene blue and reduction of 4-nitrophenol. *ACS Omega*, *7*(35), 30908–30919. https://doi.org/10.1021/acsomega.2c03006
18. Basit, R. A., Shams, S., Yasin, M., & Manzoor, U. (2023). Successive photocatalytic degradation of methylene blue by ZnO, CuO, and ZnO/CuO

synthesized from *Coriandrum sativum* plant extract via green synthesis technique. *Crystals*, *13*(2), 281. https://doi.org/10.3390/cryst13020281

19. Ouir, S., Lahmar, H., Saadi, M., & Boudabous, L. (2023). Structural, morphological and optical characterization of CuO/ZnO nanocomposite films. *Applied Physics A*, *129*(1), 10. https://doi.org/10.1007/s00339-022-06959-9
20. Renuka, L., Shubhashree, M. V., Radhakrishnan, T. S., & Rajendra, W. (2017). Synthesis of sunlight driven ZnO/CuO nanocomposite: Characterization, optical, electrochemical and photocatalytic studies. *Materials Today: Proceedings*, *4*(11), 11782–11790. https://doi.org/10.1016/j.matpr.2017.06.012
21. Gbair, G. A., & Alshamsi, H. A. (2024). Facile green synthesis of CuO-ZnO nanocomposites from *Argyreia nervosa* leaves extract for photocatalytic degradation of Rhodamine B dye. *Biomass Conversion and Biorefinery*, *14*(22), 28117–28132. https://doi.org/10.1007/s13399-024-04536-w
22. Jeevarathinam, M., & Asharani, I. (2024). Synthesis of CuO, ZnO nanoparticles, and CuO-ZnO nanocomposite for enhanced photocatalytic degradation of Rhodamine B: A comparative study. *Scientific Reports, 14*(1), 9718. https://doi.org/10.1038/s41598-024-36452-6